J Biomol NMR (2015) 61:109–121
DOI 10.1007/s10858-014-9890-7

ARTICLE

Easy and unambiguous sequential assignments of intrinsically disordered proteins by correlating the backbone ^{15}N or $^{13}C'$ chemical shifts of multiple contiguous residues in highly resolved 3D spectra

Yuichi Yoshimura · Natalia V. Kulminskaya · Frans A. A. Mulder

Received: 5 October 2014 / Accepted: 15 December 2014 / Published online: 11 January 2015

Abstract Sequential resonance assignment strategies are typically based on matching one or two chemical shifts of adjacent residues. However, resonance overlap often leads to ambiguity in resonance assignments in particular for intrinsically disordered proteins. We investigated the potential of establishing connectivity through the three-bond couplings between sequentially adjoining backbone carbonyl carbon nuclei, combined with semi-constant time chemical shift evolution, for resonance assignments of small folded and larger unfolded proteins. Extended sequential connectivity strongly lifts chemical shift degeneracy of the backbone nuclei in disordered proteins. We show here that 3D (H)N(COCO)NH and (HN)CO (CO)NH experiments with relaxation-optimized multiple pulse mixing correlate up to seven adjacent backbone amide nitrogen or carbonyl carbon nuclei, respectively, and connections across proline residues are also obtained straightforwardly. Multiple, recurrent long-range correlations with ultra-high resolution allow backbone $^{1}H^{N}$, $^{15}N^{H}$, and $^{13}C'$ resonance assignments to be completed from a single pair of 3D experiments.

Keywords Carbonyl–carbonyl J-coupling · Chemical shift degeneracy · Intrinsically disordered proteins · Homonuclear isotropic mixing · Sequential resonance assignment

Abbreviations

$^{3}J_{C'C'}$	Three-bond coupling between sequentially adjoining $^{13}C'$ nuclei
αSyn	α-Synuclein
CSA	Chemical shift anisotropy
DSS	4,4-Dimethyl-4-silapentane-1-sulfonate
IDP	Intrinsically disordered protein
MOCCA-XY16	Modified phase cycled Carr–Purcell multiple pulse sequence with XY16 supercycles
RF	Radiofrequency

Introduction

An essential first step for structural and dynamic analysis of protein NMR spectra is resonance assignments. Various types of multidimensional experiments, typically ^{1}H and ^{15}N centered triple resonance experiments which contain sequential information of backbone and side chain chemical shifts, have been developed for resonance assignments of isotopically labelled proteins (Grzesiek and Bax 1992; Ikura et al. 1990; Sattler et al. 1999). The secondary structure elements of folded proteins can be predicted by the chemical shifts obtained from the sequential assignment. Similarly, the chemical shifts in intrinsically disordered proteins (IDPs) are of significant value, since they reflect the conformational preference of polypeptide chains with atomic resolution (Camilloni et al. 2012; Kjaergaard and Poulsen 2012; Tamiola et al. 2010; Tamiola and Mulder 2012). However, unambiguous resonance assignments for IDPs are often challenging due to chemical shift degeneracy, as IDPs lack a well-defined secondary and/or

Electronic supplementary material The online version of this article (doi:10.1007/s10858-014-9890-7) contains supplementary material, which is available to authorized users.

Y. Yoshimura · N. V. Kulminskaya · F. A. A. Mulder (✉)
Department of Chemistry and Interdisciplinary Nanoscience Center (iNANO), Aarhus University, Gustav Wieds Vej 14, 8000 Aarhus C, Denmark
e-mail: fmulder@chem.au.dk

tertiary structure under physiological conditions and exist as dynamic ensembles of interconverting structures (Uversky 2011). Since IDPs play diverse and important roles in biology, such as transcriptional and translational regulation, membrane fusion and transport, and cell cycle control (Wright and Dyson 1999), and IDPs are also implicated in various human disorders (Uversky and Fink 2004), it is of significant biological relevance to study IDPs, and continuous advances in NMR techniques are therefore necessary for their structural characterization (Felli and Pierattelli 2014; Kosol et al. 2013; Mulder et al. 2010).

As chemical shifts of aliphatic ^{1}H and ^{13}C nuclei are sensitive to the secondary structure and scarcely influenced by the neighboring amino acid residues, the resonance assignment strategy and secondary structure determination in folded proteins largely rely on the dispersion of those nuclei. A set of 3D experiments, such as HNCACB and CBCA(CO)NH, give unique combinations through chemical shifts of $^{13}C^{\alpha}$ and $^{13}C^{\beta}$ nuclei in resonance assignments of folded proteins. In unfolded systems, however, those experiments show no or limited dispersion for the $^{13}C^{\alpha}$ and $^{13}C^{\beta}$ chemical shifts of the same amino acid residue in a different place in the sequence, because local anisotropic interactions are averaged out by conformational fluctuations. In particular, sequential repeats together with structural disorder cause severe resonance overlap (Motackova et al. 2010; Novacek et al. 2014). On the other hand, the backbone nitrogen ($^{15}N^{H}$) and carbonyl carbon ($^{13}C'$) chemical shifts are more sensitive to the local amino acid sequence (Schwarzinger et al. 2001; Wishart et al. 1995; Yao et al. 1997), and these nuclei have comparatively large chemical shift dispersion in IDPs (Felli and Pierattelli 2014), which is crucial for unambiguous resonance assignments of disordered proteins. As seen in Fig. 1a, the backbone $^{13}C'$–$^{15}N^{H}$ correlations exhibit favorable chemical shift dispersion. Furthermore, as nuclear spin relaxation rates for $^{15}N^{H}$ and $^{13}C'$ in unfolded systems are much lower than those in folded proteins, ultra-high resolution spectra with long acquisition times for chemical shift evolution can be recorded. In this study, we examined the use of backbone $^{15}N^{H}$ and $^{13}C'$ nuclei for sequential resonance assignments in uniformly ^{13}C, ^{15}N-labelled human α-synuclein (αSyn, 140 amino acid residues).

We investigated the potential of using the three-bond couplings between sequentially adjoining $^{13}C'$ nuclei ($^{3}J_{C'C'}$) for establishing sequential connectivity. The $^{3}J_{C'C'}$ value (in Hz) is described by the following Karplus equation (Hu and Bax 1996):

$$^{3}J_{C'C'} = 1.33\ \cos^{2}\phi - 0.88\ \cos\phi + 0.62 \quad (1)$$

where ϕ is the backbone angle involving the backbone C′–N^{H}–C^{α}–C′. The (HN)CO(CO)NH scheme, as described previously (Grzesiek and Bax 1997), utilizes homonuclear Hartmann–Hahn cross polarization to transfer $^{13}C'$ magnetization between neighbors. As seen from Fig. 1a, the relatively large chemical shift dispersion of $^{15}N^{H}$ nuclei can also be exploited. Therefore, 3D (H)N(COCO)NH experiments could prove particularly useful for sequential resonance assignments of IDPs. The magnetization transfer through the (HN)CO(CO)NH and (H)N(COCO)NH schemes can, respectively, be described as:

$$^{1}H^{N} \rightarrow {}^{15}N^{H} \rightarrow {}^{13}C'\,(t_1) \rightarrow {}^{13}C'\,(\text{mixing}) \rightarrow {}^{15}N^{H}(t_2) \rightarrow {}^{1}H^{N}(t_3) \quad (2a)$$

$$^{1}H^{N} \rightarrow {}^{15}N^{H}(t_1) \rightarrow {}^{13}C' \rightarrow {}^{13}C'\,(\text{mixing}) \rightarrow {}^{15}N^{H}(t_2) \rightarrow {}^{1}H^{N}(t_3) \quad (2b)$$

Several pulse sequences in this vein have been described for sequential resonance assignments (Balayssac et al. 2006; Bermel et al. 2006; Felli et al. 2009; Liu et al. 2000). In the following we demonstrate how these experiments can be adapted and implemented for the straightforward resonance assignments of IDPs, simultaneously yielding up to seven chemical shift correlations per residue. We demonstrate how the large number of correlations is key to lifting degeneracy for IDPs, and facilitates correlations across proline residues, which are highly abundant in IDPs.

Figure 1b, c illustrates sequential connectivity of $^{13}C'$ and $^{15}N^{H}$ nuclei obtained by these 3D experiments. In order to improve the resolution of the ^{13}C and ^{15}N dimensions relative to existing pulse schemes, both t_1 (i.e. ^{13}C and ^{15}N for (HN)CO(CO)NH and (H)N(COCO)NH, respectively) and t_2 (^{15}N) were implemented as semi-constant time chemical shift evolution periods (Grzesiek and Bax 1993; Logan et al. 1993), and ^{1}H spins were decoupled during the t_1 (^{13}C chemical shift) evolution period in the (HN)CO(CO)NH experiment as the ^{3}J couplings between side chain $^{1}H^{\beta}$ and backbone $^{13}C'$ nuclei can be up to 6 Hz, and therewith limit the resolution that can be achieved. Although the small magnitude of $^{3}J_{C'C'}$ (about 1 Hz for disordered proteins) requires an extended period for efficient coherence transfer, a modified phase cycled Carr–Purcell multiple pulse sequence with XY16 supercycles (MOCCA-XY16) allows a significant reduction of relaxation loss compared to other isotropic homonuclear mixing sequences (Furrer et al. 2004; Kramer et al. 2001). An extremely long (>500 ms) isotropic mixing with the MOCCA-XY16 sequence established the connectivity of up to seven residues $i, i \pm 1, i \pm 2$, and $i \pm 3$, which strongly lifts chemical shift degeneracy of the backbone nuclei in disordered proteins (see below).

The strategy proposed in this article allowed sequential resonance assignment for unfolded systems from 3D experiments at a protein concentration of ~0.2 mM

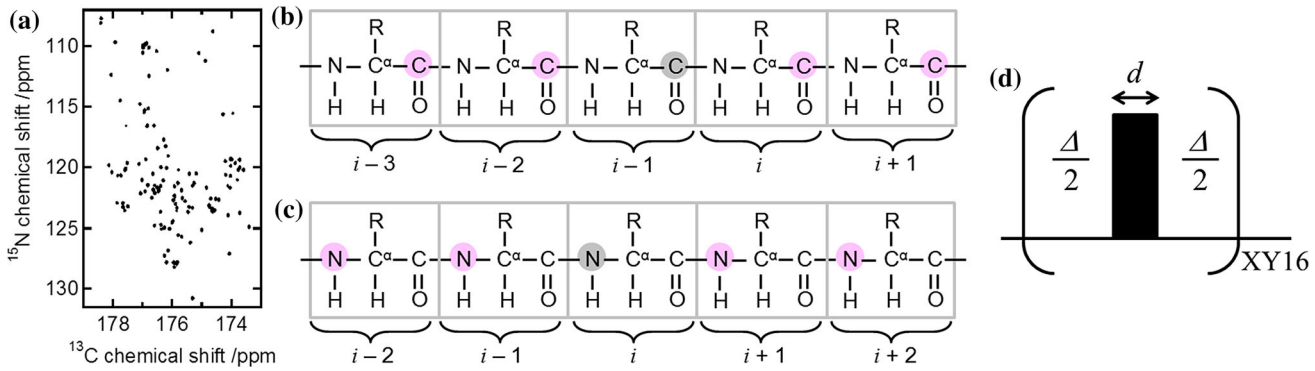

Fig. 1 **a** 2D ^{15}N–^{13}C projection of the 3D HNCO spectrum of uniformly ^{13}C,^{15}N-labelled αSyn. The horizontal and vertical scales are comparable in the unit of Hz. The average natural line width at half height for 96 well-resolved resonances of αSyn in the HNCO spectrum is 3.63 ± 1.03 Hz for ^{13}C′ and 4.14 ± 1.55 Hz for ^{15}N^{H}. **b**, **c** Sequential connectivity of ^{13}C′ (**b**) and ^{15}N^{H} (**c**) nuclei, obtained by 3D (HN)CO(CO)NH (**b**) and (H)N(COCO)NH (**c**) experiments, respectively. The 3D (HN)CO(CO)NH experiment provides a "diagonal" resonance ($^{13}C_{i-1}$, *grey*) and cross resonances ($^{13}C_{i-3}$, $^{13}C_{i-2}$, $^{13}C_{i}$, and $^{13}C_{i+1}$, *purple*) in the ω_1 dimensions in the strip plot of the amide group of residue *i* with the $^{15}N_i$ (ω_2) and $^{1}H_i$ (ω_3) frequencies, whereas the 3D (H)N(COCO)NH experiment provides a diagonal resonance ($^{15}N_i$, *grey*) and cross resonances ($^{15}N_{i-2}$, $^{15}N_{i-1}$, $^{15}N_{i+1}$, and $^{15}N_{i+2}$, *purple*) in the ω_1 dimensions in a strip plot of the amide group of residue *i*. Although side chain amide groups of asparagine residues are also correlated in these experiments through the intra-residue ^{3}J couplings between side chain $^{13}C^{\gamma}$ and backbone ^{13}C′ nuclei, it should be noted that only the amide groups within which one of the two amide protons is substituted with a deuteron (^{15}NHD) lead to signal, and that those resonances are therefore relatively weak. **d** Basic building block of MOCCA-XY16. The supercycle of the phase of the RF pulse for XY16 is: *x*, *y*, *x*, *y*, *y*, *x*, *y*, *x*, −*x*, −*y*, −*x*, −*y*, −*y*, −*x*, −*y*, −*x*

without the use of a cryogenic probehead. Although several 4D and 5D NMR experiments have been implemented for resonance assignments of IDPs in order to eliminate spectral overlap caused by amino acid repetition and a high number of resonances in larger IDPs (for example, Bermel et al. 2012; Motackova et al. 2010), working with 3D data is highly intuitive, and processing and data manipulations are easy and fast.

Finally, although the approach presented here is particularly well-suited for IDPs, it can also be employed for resonance assignments of globular proteins rich in β-strands because of the larger $^{3}J_{C'C'}$ value for extended structures ($^{3}J_{C'C'}$ = 1.4–2.4 Hz when ϕ = −120° to −150°). Therefore, we also tested the pulse sequences with uniformly ^{13}C, ^{15}N-labelled human ubiquitin (76 amino acid residues). Bruker pulse sequence code for the 3D (H)N(COCO)NH and (HN)CO(CO)NH experiments is provided in the Supplementary Material, and at http://www.protein-nmr.org. Pulse sequence updates will be posted on the website.

Materials and methods

Sample preparation

Expression and purification of uniformly ^{13}C,^{15}N-labelled αSyn was described previously (Giehm et al. 2011), with the exception that *E. coli* was grown in M9 minimal medium supplemented with ^{15}N-labelled NH_4Cl and ^{13}C-labelled D-glucose. Lyophilized αSyn was dissolved at a protein concentration of 170 μM in 4 mM sodium 2-(*N*-morpholino)ethanesulfonate (MES) at pH 5.6. The sample solution contains 10 % (v/v) D_2O for field lock and 100 μM sodium 4,4-dimethyl-4-silapentane-1-sulfonate (DSS) as chemical shift reference (Markley et al. 1998).

NMR experiments

Unless otherwise indicated, NMR experiments were performed at 298 K on a Bruker Avance NMR spectrometer at ^{1}H frequency of 500 MHz (i.e. at the magnetic field of 11.7 T). The ^{1}H and ^{15}N carrier frequencies were placed at 4.7 and 119 ppm, respectively. The pulses for excitation of ^{13}C′ and $^{13}C^{\alpha}$ centered at 176 and 54 ppm, respectively. The pulse sequences were first tested on uniformly ^{13}C,^{15}N-labelled human ubiquitin (2 mM) before the experiments were performed on uniformly ^{13}C,^{15}N-labelled αSyn.

In order to improve the resolution of the ^{15}N dimension in 3D HNCO (Kay et al. 1994), (H)N(COCO)NH, and (HN)CO(CO)NH experiments, t_2 was implemented as a semi-constant time evolution period (Grzesiek and Bax 1993; Logan et al. 1993). Additional gradient pulses were included during the reverse INEPT step to remove off-resonance dependent mixed-phase artifacts (Mulder et al. 2011). In the HNCO and (HN)CO(CO)NH experiments, ^{1}H spins were decoupled during the t_1 (^{13}C chemical shift) evolution period. In the (HN)CO(CO)NH and (H)N(COCO)NH experiments, t_1 (i.e. ^{13}C and ^{15}N dimensions, respectively) was also extended by semi-constant time chemical shift evolution. The radiofrequency (RF) field of

the 180° pulses in MOCCA-XY16 was set at 8.64 kHz with a duration of the 180° pulse (*d*) of 57.9 μs, which was determined such that $^{13}C^{\alpha}$ nuclei experience an effective 360° rotation during each carbonyl 180° pulse (Felli et al. 2009). The delays between the 180° pulses (Δ) were set at 500 μs. The MOCCA-XY16 scheme is illustrated in Fig. 1d, and the pulse sequences of the 3D (HN)CO(CO)NH and (H)N(COCO)NH experiments are shown in Fig. 2. As discussed below, the temperature increase during the experiment was measured by monitoring the ^{1}H chemical shift of HOD in D_2O containing 250 μM DSS as chemical shift reference.

The NMR spectra of αSyn were recorded with spectral widths of 16 ppm (8.01 kHz), 25 ppm (1.27 kHz), and 6 ppm (0.75 kHz) for ^{1}H, ^{15}N, and ^{13}C, respectively. The HNCO spectrum was collected with a matrix size of 1,024 (^{1}H, t_3) × 96 (^{15}N, t_2) × 96 (^{13}C, t_1) complex points. The 3D (H)N(COCO)NH and (HN)CO(CO)NH spectra were collected with a matrix size of 768 (^{1}H, t_3) × 108 (^{15}N, t_2) × 108 (^{15}N, t_1) and 768 (^{1}H, t_3) × 108 (^{15}N, t_2) × 96 (^{13}C, t_1) complex points, respectively. All NMR data were processed using nmrPipe (Delaglio et al. 1995) and analyzed with Sparky (Goddard and Kneller SPARKY 3, University of California, San Francisco).

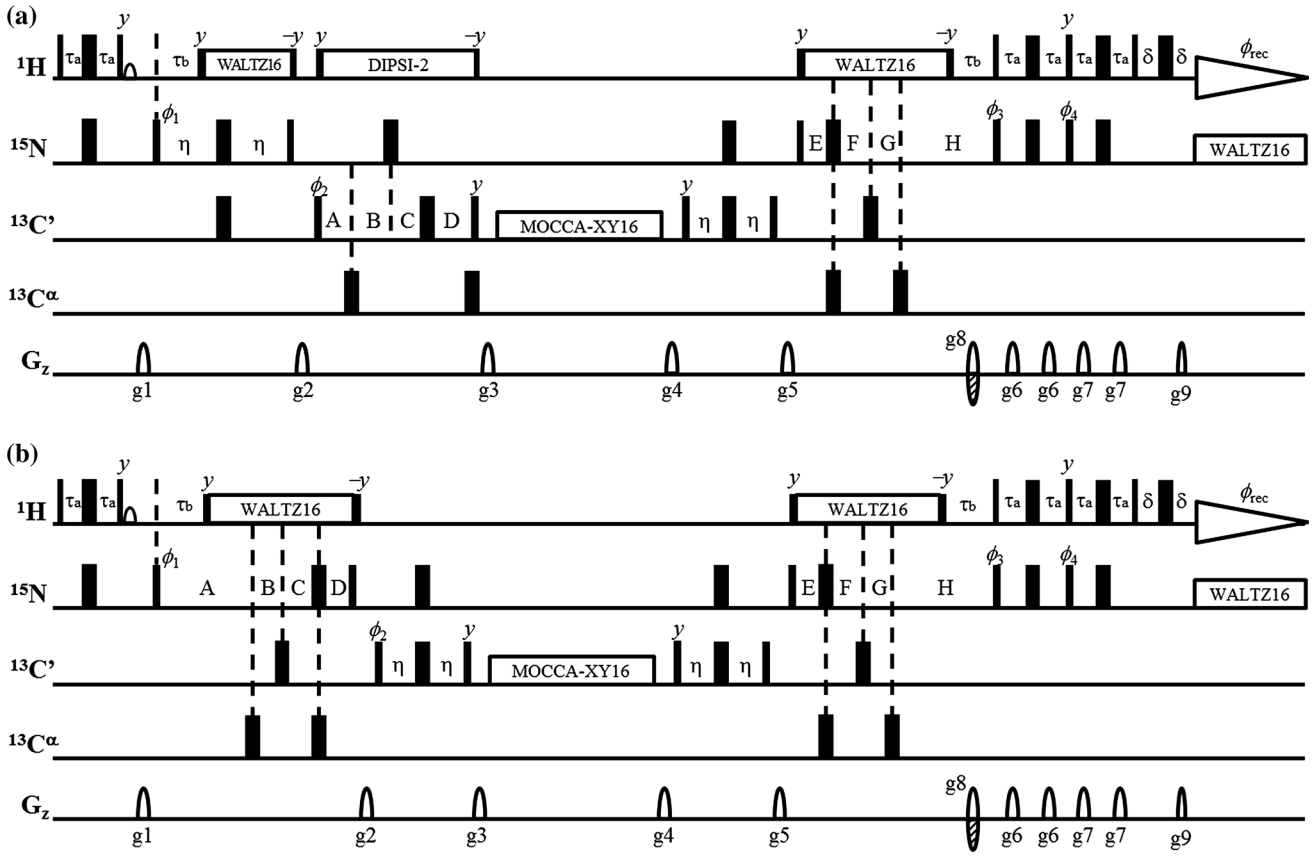

Fig. 2 Pulse sequences for the 3D (HN)CO(CO)NH (**a**) and (H)N(COCO)NH (**b**) experiments. The *narrow* and *wide bars* represent 90° and 180° pulses, respectively. Unless otherwise indicated, the pulses are applied with phase *x*. A water flip-back pulse for a duration of 1 ms to selectively rotate the magnetization of solvent is included in order to minimize saturation of the H_2O signal (Kay et al. 1994). The delays used are: $\tau_a = 2.7$ ms, $\tau_b = 5.5$ ms, $\eta = 13.5$ ms, and $\delta = 0.31$ ms. The durations of the sine-shaped z-axis pulsed field gradients are 1.0 ms for *g1–g8*, and 0.101 ms for *g9*. The strengths of the gradients (in G/cm) are: g1, 15.9; g2, 10.6; g3, 18.5; g4, 23.8; g5, 14.8; g6, 31.7; g7, 6.3; g8, 42.3; g9, 42.3. The phase cycles employed are: $\phi_1 = \{x\}$, $\phi_2 = \{x, -x\}$, $\phi_3 = \{x, x, -x, -x\}$, $\phi_4 = \{-y, -y, y, y\}$, and $\phi_{rec} = \{x, -x, -x, x\}$. **a** the values of the delays containing t_1 for the *n*-th data point are: $A = n{\cdot}\Delta t/2$, $B = \eta$, $C = (1 - n/N){\cdot}\eta$, and $D = n{\cdot}(\Delta t/2 - \eta/N)$, where Δt is the dwell time and *N* is the index of the last data point. Quadrature detection in the t_1 (^{13}C) dimension is achieved with States-TPPI (Marion et al. 1989), where the phase ϕ_2 is increased by 90°. **b** the values of the delays containing t_1 for the *n*-th data point are: $A = \eta + n{\cdot}(\Delta t/2 - \eta/N)$, $B = (n/N){\cdot}\eta$, $C = n{\cdot}(\Delta t/2 - \eta/N)$, and $D = (1 - n/N){\cdot}\eta$. Quadrature detection in the t_1 (^{15}N) dimension is achieved with States-TPPI, where the phase ϕ_1 is increased by 90°. In both **a** and **b**, the values of the delays containing t_2 for the *n*-th data point are: $E = (1 - n/N){\cdot}\eta$, $F = n{\cdot}(\Delta t/2 - \eta/N)$, $G = (n/N){\cdot}\eta$, and $H = \eta + n{\cdot}(\Delta t/2 - \eta/N)$. For each value of t_2, N- and P-type coherences are obtained by recording two data sets, whereby the sign of the gradient *g8* and the phase ϕ_4 are inverted for the second set, and processed to generate pure absorption mode lineshapes in the ^{15}N dimension (Kay et al. 1992). The pulse sequence code for Bruker spectrometers is provided in the Supplementary Material

Results and discussion

Carbonyl–carbonyl correlations for resonance assignments of IDPs

We investigated the usefulness of carbonyl–carbonyl correlation experiments such as 3D (HN)CO(CO)NH (Grzesiek and Bax 1997) and (H)N(COCO)NH (Liu et al. 2000) schemes for sequential resonance assignments of disordered proteins. Figure 3 shows the dependency of chemical shift degeneracies in the resonance assignments of αSyn on the resolution of $^{15}N^{H}$ and $^{13}C'$ chemical shifts. The HNCO (Kay et al. 1994) and HN(CA)CO (Clubb et al. 1992) schemes are common 3D experiments which correlate the carbonyl carbon of residues $i-1$ and i for a given amide strip plot of the i-th residue. The resonances of interest can be uniquely matched in the sequential assignment without chemical shift degeneracy only where there is no other resonance within a range of a certain chemical shift tolerance. In the unfolded system, high chemical shift degeneracy makes the sequential resonance assignments very difficult. For example, only 11 % of the $^{13}C'$ chemical shifts of αSyn are uniquely matched even with a tolerance of as small as 0.04 ppm (i.e. 5.03 Hz at the magnetic field of 11.7 T). However, an additional matching chemical shift dramatically lifts the chemical shift degeneracy for unfolded proteins.

This can be achieved in the (HN)CO(CO)NH experiments, where the magnetization is transferred from a $^{13}C'$ nucleus to sequentially adjoining $^{13}C'$ nuclei via $^{3}J_{C'C'}$ couplings (Fig. 1b). Here, it is assumed for simplicity that the carbonyl magnetization is transferred to only neighboring carbonyl nuclei, though an extended isotropic mixing period may correlate more than three carbonyl carbon nuclei (see below). The $^{13}C'$ magnetization which is not transferred to its $^{13}C'$ neighbors during the isotropic mixing period will give rise to a "diagonal" resonance with the $^{13}C_{i-1}$, $^{15}N_i$, and $^{1}H_i$ frequencies in ω_1, ω_2, and ω_3 dimensions, respectively, whereas two cross resonances with $^{13}C_{i-2}$ and $^{13}C_i$ frequencies also appear in a strip plot of the amide group of residue i. Now, 85 % of the $^{13}C'$ chemical shifts of αSyn are uniquely matched with a tolerance of 0.04 ppm (Fig. 3a). The resonances with such a small tolerance can be obtained by recording the spectrum with ultra-high resolution. As transverse spin relaxation rates of $^{13}C'$ nuclei in highly disordered molecules are very low, ultra-high resolution spectra can be recorded with a long acquisition period for $^{13}C'$ chemical shift evolution. The average natural line width at half height for αSyn is 3.6 Hz (i.e. 0.029 ppm at 11.7 T). In order to provide adequate resolution of the chemical shifts, the acquisition time can be extended by semi-constant time chemical shift evolution, and in the (HN)CO(CO)NH experiment, ^{1}H spins were decoupled during the t_1 (^{13}C chemical shift) evolution period (Fig. 2a).

Similarly, $^{15}N^{H}$ nuclei also have comparatively large chemical shift dispersion with long transverse spin relaxation time in IDPs. The (H)N(COCO)NH scheme provides a diagonal resonance with the $^{15}N_i$ and two cross resonances with $^{15}N_{i-1}$ and $^{15}N_{i+1}$ frequencies in the strip plot of the i-th amide group (Fig. 1c). A tolerance of 0.1 ppm yielded 87 % of the $^{15}N^{H}$ resonances of αSyn with unique matching (Fig. 3a). The average natural line width at half height for αSyn is 4.1 Hz (i.e. 0.082 ppm for 11.7 T). For comparison of the use of $^{13}C'$ and $^{15}N^{H}$ nuclei, chemical shift resolution in the Hz unit was shown in Fig. 3b, given that the magnetic

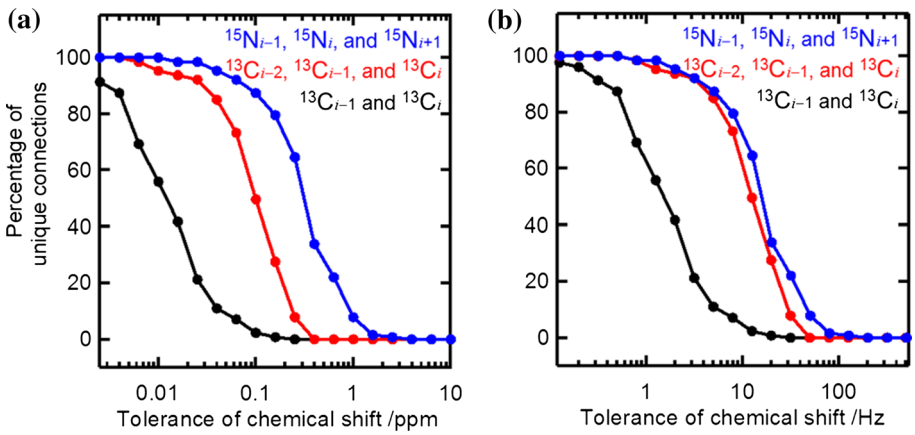

Fig. 3 Dependence of degeneracies in the resonance assignments of αSyn on chemical shift resolution. The *black lines* were obtained assuming that only two matching chemical shifts (i.e. $^{13}C_{i-1}$ and $^{13}C_i$) are available, while the *red* and *blue lines* were obtained by using three matching chemical shifts (i.e. $^{13}C_{i-2}$, $^{13}C_{i-1}$ and $^{13}C_i$ for $^{13}C'$ correlations and $^{15}N_{i-1}$, $^{15}N_i$ and $^{15}N_{i+1}$ for $^{15}N^{H}$ correlations, respectively). **a** the percentage of unique connections was plotted against tolerance in the unit of ppm. **b** the *horizontal axis* was shown in the Hz unit for comparison of the use of $^{13}C'$ and $^{15}N^{H}$ nuclei, given that the magnetic field strength is 11.7 T (i.e. ^{1}H frequency of 500 MHz)

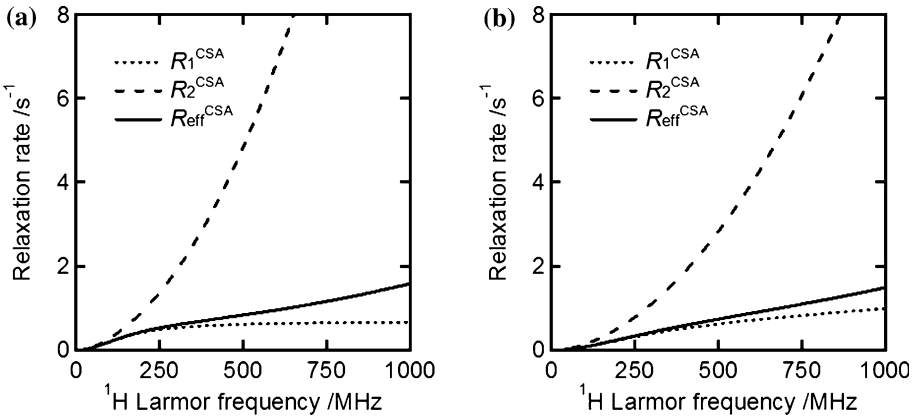

Fig. 4 Dependence of longitudinal (R_1^{CSA}), transverse (R_2^{CSA}), and effective (R_{eff}) relaxation contributions due to $^{13}C'$ CSA on magnetic field strengths during the MOCCA-XY16 mixing period for a folded protein (**a**) and an IDP (**b**)

field strength is 11.7 T (a ^{1}H frequency of 500 MHz). Because of the large chemical shift dispersion of $^{15}N^H$ nuclei compared to $^{13}C'$ nuclei (Fig. 1a), $^{15}N^H$ correlations provided larger number of resonances with unique matching.

Effective $^{13}C'$ relaxation during the MOCCA-XY16 mixing period

As the $^3J_{C'C'}$ values are very small (i.e. $\sim$1 Hz), a relatively long mixing period is required for coherence transfer through backbone $^{13}C'$ nuclei. In order to achieve efficient transfer of the $^{13}C'$ magnetization, suppression of relaxation loss is a critical issue. As described previously (Furrer et al. 2004; Kramer et al. 2001), the MOCCA-XY16 scheme allows a significant reduction of relaxation loss compared to other isotropic homonuclear mixing sequences as the magnetization is kept longitudinal during the trajectory between the 180° pulses. We estimated the dependence of the effective $^{13}C'$ relaxation rate on the magnetic field strength. Here, the contributions of various dipole–dipole interactions between the $^{13}C'$ spins and adjacent spins are neglected because the relaxation of the backbone $^{13}C'$ in proteins is dominated by chemical shift anisotropy (CSA) (Engelke and Ruterjans 1997). The longitudinal (R_1^{CSA}) and transverse (R_2^{CSA}) relaxation contributions due to the $^{13}C'$ CSA are, respectively, given by:

$$R_1^{CSA} = \frac{1}{3}\Delta\delta_g^2\gamma_C^2 B_0^2 J(\omega_C) \tag{3a}$$

$$R_2^{CSA} = \frac{1}{18}\Delta\delta_g^2\gamma_C^2 B_0^2 (4J(0) + 3J(\omega_C)) \tag{3b}$$

where $\Delta\delta_g$ is the generalized CSA coupling constant, γ_C is the gyromagnetic ratio of the ^{13}C nucleus, B_0 is the magnetic field strength, and $J(\omega)$ is the spectral density function. The effective relaxation rate due to $^{13}C'$ CSA during the mixing sequence (R_{eff}) is estimated by:

$$R_{eff} = w_1 R_1^{CSA} + w_2 R_2^{CSA} \tag{4}$$

where w_1 and w_2 are the longitudinal and transverse weights during the MOCCA-XY16 mixing period, and $w_1 + w_2 = 1$. When $\Delta/d = 8.64$ and the off-resonance effect on w_1 and w_2 is ignored, $w_1 = 0.948$ and $w_2 = 0.052$. Although the $^{13}C'$ CSA in proteins varies from 140 to 146 ppm (Markwick and Sattler 2004), the value was fixed at 143 ppm. The spectral density function used in the model free approach (Lipari and Szabo 1982a, b) is described as:

$$J(\omega) = \frac{2}{5}\left[\frac{S^2\tau_m}{1+(\omega\tau_m)^2} + \frac{(1-S^2)\tau}{1+(\omega\tau)^2}\right] \tag{5}$$

where S^2 is the generalized order parameter, $\tau^{-1} = \tau_e^{-1} + \tau_m^{-1}$, and τ_m and τ_e are the correlation times for overall tumbling and internal motion, respectively. Figure 4a shows the R_{eff} rate as a function of the magnetic field strength for small folded proteins (e.g. ubiquitin). For simplicity, the fast internal motion is ignored (i.e. $S^2 = 1$) and $\tau_m = 4$ ns. For analyzing dynamics of unfolded proteins, on the other hand, the Cole–Cole distribution function is used to incorporate distributions of correlation times in the model free analysis (Buevich and Baum 1999):

$$J(\omega) = \frac{1}{5}\left[\frac{1}{\omega}\frac{S^2\cos\left[\frac{\pi}{2}(1-\varepsilon)\right]}{\cosh[\varepsilon\ln(\omega\tau_0)] + \sin\left[\frac{\pi}{2}(1-\varepsilon)\right]} + \frac{2(1-S^2)\tau}{1+(\omega\tau)^2}\right] \tag{6}$$

where τ_0 and ε are the mean value and the width of the Cole–Cole distribution function, respectively, and $\tau^{-1} = \tau_0^{-1} + \tau_m^{-1}$. Figure 4b shows the dependence of the R_{eff} rate on the magnetic field strength for IDPs (e.g. αSyn). Here, it is assumed that $\tau_0 = 2$ ns, $\varepsilon = 0.97$, $\tau_e = 100$ ps, and $S^2 = 0.6$ (Buevich and Baum 1999). Because Eq. 6 is not defined at $\omega = 0$ rad/s, it is also assumed that the $J(0)$ value in Eq. 3b is equal to the value at $J(1$ rad/s), given that all interconversion processes are much faster than 1 rad/s (Buevich et al. 2001). As seen from Fig. 5, efficient transfer of the $^{13}C'$ magnetization during an extended

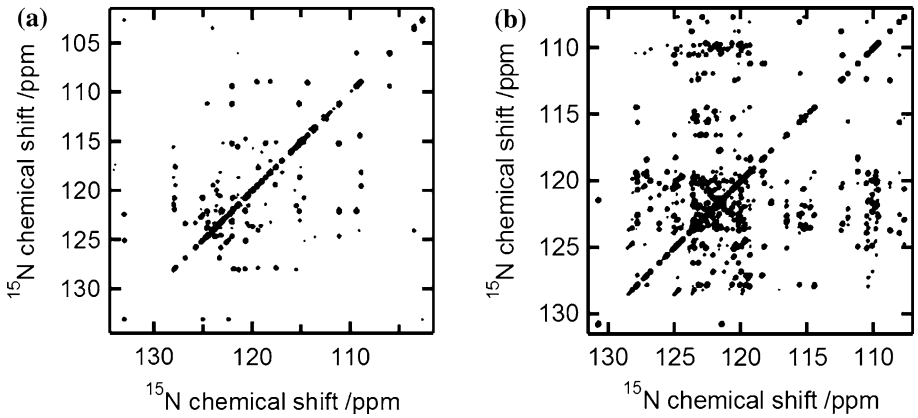

Fig. 5 2D ^{15}N–^{15}N projection of the 3D (H)N(COCO)NH spectra of uniformly ^{13}C,^{15}N-labelled ubiquitin (**a**) and αSyn (**b**) with MOCCA-XY16 isotropic mixing at the magnetic field of 11.7 T. The mixing periods are 500 and 393 ms for ubiquitin and αSyn, respectively

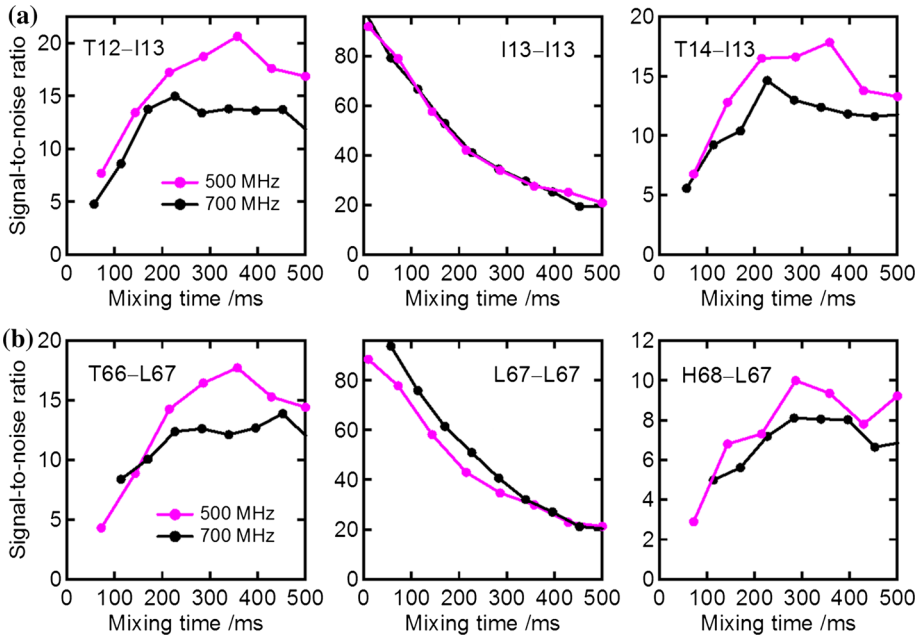

Fig. 6 Carbonyl–carbonyl transfer efficiency of the MOCCA-XY16 schemes at the magnetic field of 11.7 T (*purple*) and 17.6 T (*black*). A series of 2D (H)N(COCO)(N)H spectra with different mixing periods were recorded on uniformly ^{13}C,^{15}N-labelled ubiquitin, and the signal-to-noise ratio for amino acid residues of $i - 1$ (*left*), i (*middle*), and $i + 1$ (*right*) are plotted against the ^{13}C′ mixing periods. The duration of the 180° pulse (d) and the delay between the 180° pulses (Δ) were $d = 57.9$ and 41.4 μs and $\Delta = 500$ and 400 μs at 11.7 and 17.6 T, respectively. **a** Correlations of T12–I13, I13–I13, and T14–I13. **b** Correlations of T66–L67, L67–L67, and H68–L67

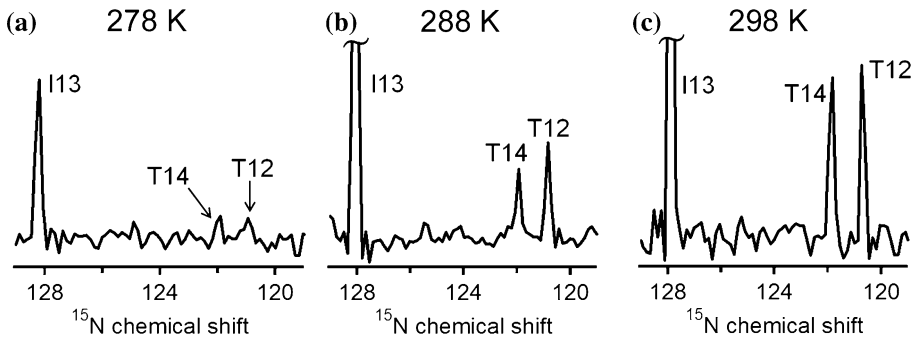

Fig. 7 Traces from 2D (H)N(COCO)(N)H spectra with the MOCCA-XY16 mixing period of 278.8 ms recorded on uniformly ^{13}C,^{15}N-labelled ubiquitin at 278 (**a**), 288 (**b**), and 298 K (**c**). The experiments were performed on a Bruker 950 MHz spectrometer equipped with a cryogenic probe. The duration of the 180° pulse was 30.5 μs, and the delay between the 180° pulses was 260 μs. The ^{1}H^{N} chemical shifts of I13 at 278, 288, and 298 K are 9.648, 9.618, and 9.585 ppm, respectively

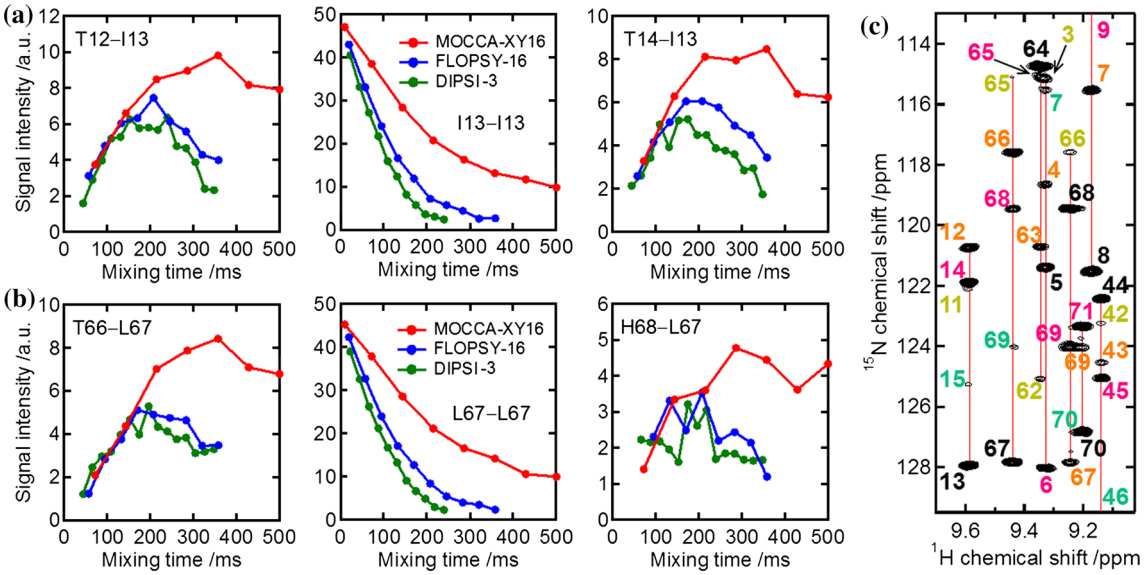

Fig. 8 Carbonyl–carbonyl transfer efficiency of MOCCA-XY16, FLOPSY-16, and DIPSI-3 schemes at the magnetic field of 11.7 T. A series of 2D (H)N(COCO)(N)H spectra were recorded on uniformly ^{13}C,^{15}N-labelled ubiquitin with different isotropic mixing periods. (**a**, **b**) Signal intensity for amino acid residues of $i - 1$ (*left*), i (*middle*), and $i + 1$ (*right*) plotted against the ^{13}C′ mixing periods with MOCCA-XY16 (*red*), FLOPSY-16 (*blue*), and DIPSI-3 (*green*). The RF amplitude of carbonyl isotropic mixing using DIPSI-3 and FLOPSY-16 was 2.50 kHz (i.e. a 90° pulse of 100 μs). For MOCCA-XY16, $d = 57.9$ and $\Delta = 500$ μs. **c** A zoomed region of the 2D (H)N(COCO)(N)H spectrum with MOCCA-XY16 for 500 ms mixing time. The numbers labelled on the spectrum indicate the amino acid residues of $i - 2$ (*yellow*), $i - 1$ (*orange*), i (*black*), $i + 1$ (*pink*), and $i + 2$ (*green*)

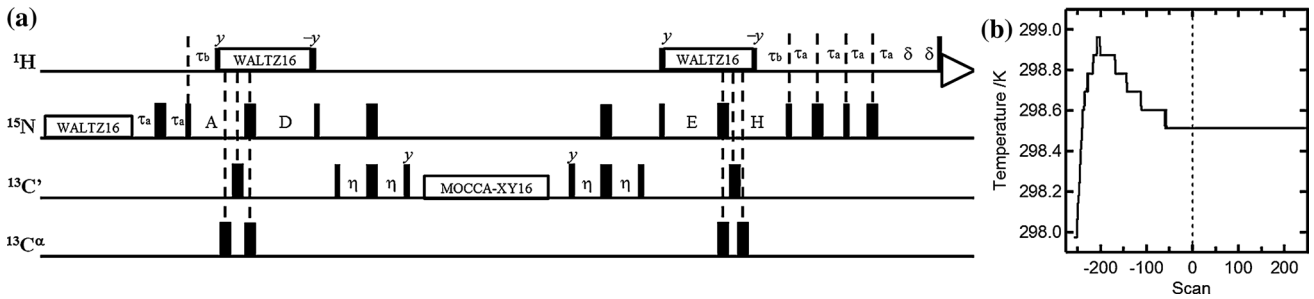

Fig. 9 Heating of the sample caused by long isotropic mixing with the MOCCA-XY16 sequence. **a** The pulse scheme to measure the temperature increase by monitoring the ^{1}H chemical shift of HOD in D_2O using a modified version of the pulse sequence in Fig. 2b. The pulse sequence starts with ^{15}N decoupling. The hard ^{1}H pulses were removed from the original pulse scheme, and instead a short pulse with a small tilt angle (~15°) was added before 1-s acquisition of the ^{1}H free induction decay. The delays used are: $\tau_a = 2.7$ ms, $\tau_b = 5.5$ ms, $\eta = 13.5$ ms, and $\delta = 0.31$ ms. The delays A, D, E, and H are equal to η (i.e. 13.5 ms), and the measurement was executed as a pseudo-2D acquisition. **b** Temperature increase with the MOCCA-XY16 mixing period of 500 ms

mixing period can be achieved, demonstrating that the relaxation loss is efficiently suppressed due to the reduced weight of transverse magnetization for both folded and disordered proteins.

Although R_{eff} increases at higher magnetic fields, it does go only slowly, as R_1^{CSA} becomes constant in the large molecular weight limit ($\omega_C\tau_m \gg 1$) for a rigid rotor, or increases slowly in the case of a flexible chain. For ubiquitin, the R_{eff} rates are 0.84 and 1.1 s^{-1} at $B_0 = 11.7$ and 17.6 T (i.e. the ^{1}H frequency of 500 and 700 MHz), respectively (Fig. 4a). For IDPs, the R_{eff} rates are 0.74 and 1.0 s^{-1} at 500 and 700 MHz, respectively (Fig. 4b). We investigated the magnetization transfer efficiency of the MOCCA-XY16 mixing scheme at $B_0 = 11.7$ and 17.6 T. In order to save time, a series of 2D (H)N(COCO)(N)H experiments with different mixing periods were performed instead of 3D experiments. Here, we used uniformly ^{13}C,^{15}N-labelled ubiquitin to obtain well-resolved resonances from the series of 2D experiments. In Fig. 6, the changes in the signal intensity for I13 (Fig. 6a) and L67 (Fig. 6b) and their neighboring residues, plotted against the mixing period, are shown as examples. As seen from

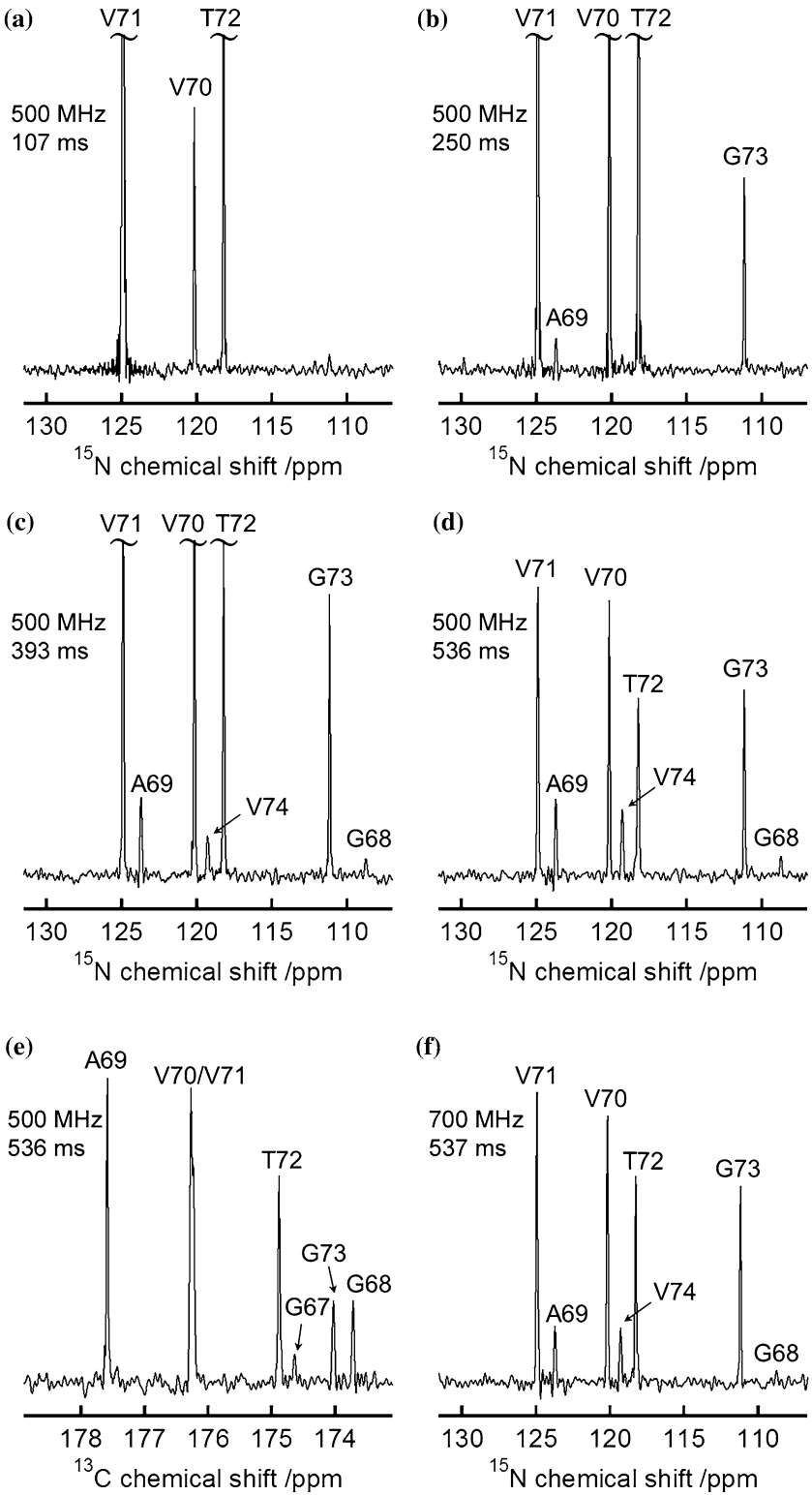

Fig. 10 Traces from 3D (H)N(COCO)NH and (HN)CO(CO)NH spectra of uniformly ^{13}C,^{15}N-labelled αSyn recorded with MOCCA-XY16 isotropic mixing. The $^{15}N^{H}$ (ω_2) and $^{1}H^{N}$ (ω_3) chemical shifts of V71 are 124.92 ppm and 8.33 ppm, respectively. **a**–**d** Traces extracted from a series of 3D (H)N(COCO)NH spectra recorded at the magnetic field of 11.7 T with the mixing periods of 107 (**a**), 250 (**b**), 393 (**c**), and 536 (**d**) ms. **e** A trace extracted from the 3D (HN)CO(CO)NH spectrum at the magnetic field of 11.7 T with the mixing period of 536 ms. **f** A traces extracted from the 3D (HN)CO(CO)NH spectrum at the magnetic field of 17.6 T with the mixing period of 537 ms

Fig. 6, the $^{13}C'$ magnetization is more efficiently transferred at the magnetic field of 11.7 T than 17.6 T, but the experiment also works well at high field, where spectral resolution is higher.

Since high field NMR is advantageous to resolve spectral overlap in particular for larger proteins, we performed the 2D (H)N(COCO)(N)H experiments at $B_0 = 22.3$ T (i.e. ^{1}H frequency of 950 MHz) as well. For folded proteins, the

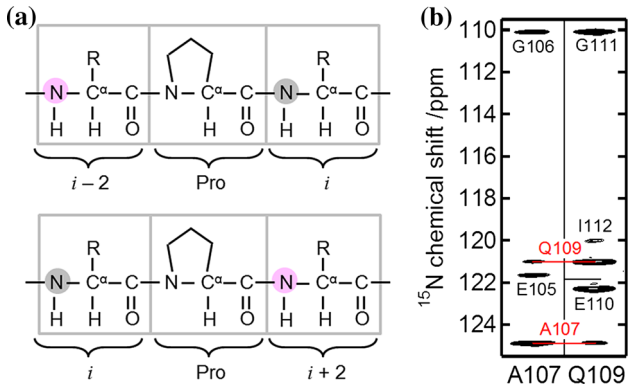

Fig. 11 **a** Schematic representation of the sequential connectivity of ^{15}N nuclei obtained by 3D (H)N(COCO)NH experiments across a proline residue. The $^{15}N^{H}$ nuclei provide diagonal (*grey*) and cross (*purple*) resonances in the ω_1 dimension in the strip plot of the amide group of residue *i* with the $^{15}N_i$ (ω_2) and $^{1}H_i$ (ω_3) frequencies. **b** Strip plots for A107 and Q109 of uniformly ^{13}C,^{15}N-labelled αSyn from 3D (H)N(COCO)NH experiments at the magnetic field of 11.7 T with MOCCA-XY16 isotropic mixing for 536 ms

overall correlation time (τ_c) becomes longer as the molecular weight becomes larger. In order to investigate the dependence of overall correlation times on the ^{13}C homonuclear magnetization transfer, the 2D spectra were recorded on ubiquitin at 298, 288, and 278 K, where the τ_c values are 4.1, 5.4, and 8.35 ns, respectively (Chang and Tjandra 2005; Wang et al. 2003). As seen from Fig. 7, the ^{13}C magnetization is efficiently transferred at 288 and 298 K. However, the magnetization transfer becomes less efficient at 278 K, suggesting that the strategy proposed in this article might be difficult to apply for resonance assignments of large folded proteins. For highly disordered proteins, on the other hand, the $^{13}C'$ and $^{15}N^{H}$ line widths are small because of the small rotational correlation time, and the resonance overlap is likely to stem from relatively broad $^{1}H^{N}$ line width due to $^{1}H^{N}$–$^{1}H^{\alpha}$ ^{3}J couplings (∼7 Hz). In this case, band-selective homonuclear ^{1}H decoupling during the acquisition period (Ying et al. 2014) or perdeuteration of proteins improve spectral resolution, although the latter gives rise to ^{2}H isotope shifts (Maltsev et al. 2012).

Carbonyl–carbonyl transfer efficiency of different isotropic mixing sequences

A series of 2D (H)N(COCO)(N)H spectra were recorded on ubiquitin to estimate the magnetization transfer efficiency of different isotropic mixing sequences. Figure 8 shows the advantage of the use of MOCCA-XY16 compared to other conventional isotropic mixing sequences, i.e. DIPSI-3 (Shaka et al. 1988) and FLOPSY-16 (Kadkhodaie et al. 1991). As expected (Felli et al. 2009), the results clearly demonstrated that the MOCCA-XY16 scheme reduces relaxation loss compared to the other mixing schemes (Fig. 8a, b). The maximum signal strength for cross resonances (N_{i-1} and N_{i+1}) was obtained with DIPSI-3 and FLOPSY-16 mixing periods of ∼200 ms, while the MOCCA-XY16 mixing scheme provided stronger signals with the mixing period of around 350 ms. Furthermore, additional resonances ($^{15}N_{i-2}$ and $^{15}N_{i+2}$) are correlated by the experiment with the MOCCA-XY16 isotropic mixing scheme for 500 ms (Fig. 8c), which would be a significant advantage to lift chemical shift degeneracy of IDPs (see below).

Since an extremely long isotropic mixing with the MOCCA-XY16 sequence potentially causes sample heating, we measured the temperature increase by monitoring the ^{1}H chemical shift of HOD in D_2O containing 250 μM DSS as chemical shift reference. The pulse scheme based on Fig. 2b was modified as shown in Fig. 9a. Briefly, hard ^{1}H pulses are removed from the original pulse scheme, and the pulse sequence starts with ^{15}N decoupling. In order to detect the ^{1}H resonances of HOD and DSS, a short pulse with a small tilt angle (∼15°) is followed by 1 s acquisition. The ^{1}H chemical shift value of HOD was obtained for each scan, and used to determine the temperature. Figure 9b shows the temperature increase with the MOCCA-XY16 mixing period of 500 ms, demonstrating that the system reached equilibrium during the dummy scans (i.e. pre-data collection scans). Although the temperature increase of the sample was modest (∼0.5 °C), it could be adjusted by adjusting the temperature regulation unit (Yuwen and Skrynnikov 2014a, b).

Correlation of the backbone chemical shifts of up to seven contiguous residues

A significant advantage of the use of $^{3}J_{C'C'}$ couplings with MOCCA-XY16 isotropic mixing sequence for resonance assignments was investigated on uniformly ^{13}C,^{15}N-labelled αSyn. Figure 10 shows traces from 3D (H)N(COCO)NH and (HN)CO(CO)NH experiments taken through the $^{15}N^{H}$ (ω_2) and $^{1}H^{N}$ (ω_3) chemical shifts for V71. A series of 3D (H)N(COCO)NH spectra with different isotorpic mixing periods (i.e. 107, 250, 393, and 536 ms) was recorded at 11.7 T (Fig. 10a–d). With a mixing period of 107 ms, the magnetization is transferred from a carbonyl to sequentially succeeding carbonyl nuclei via $^{3}J_{C'C'}$ couplings (Fig. 10a). The $^{13}C'$ magnetization which is not transferred to its $^{13}C'$ neighbors during the isotropic mixing period results in a diagonal resonance with the $^{15}N_i$, $^{15}N_i$, and $^{1}H_i$ frequencies in ω_1, ω_2, and ω_3 dimensions, respectively, whereas two cross resonances with $^{15}N_{i-1}$ and $^{15}N_{i+1}$ frequencies appear in the extracted trace of the amide group of residue *i*.

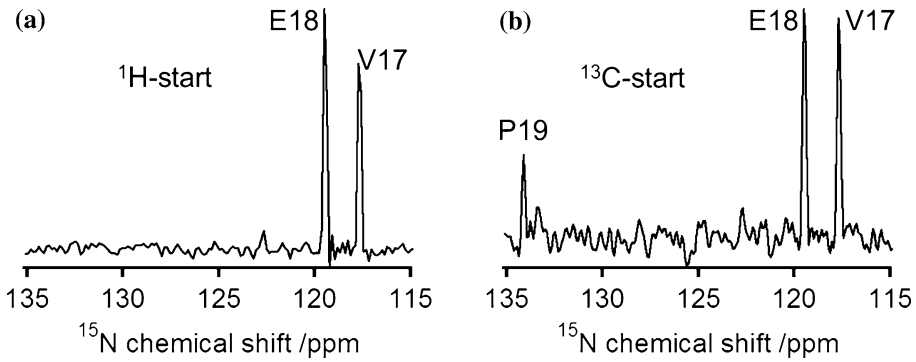

Fig. 12 Comparison of the experiments starting with ^{1}H (**a**) and ^{13}C (**b**) excitation. The experiments were performed on uniformly ^{13}C,^{15}N-labelled ubiquitin. The experiments were performed at 298 K on a Bruker 950 MHz spectrometer equipped with a cryogenic probe. The MOCCA-XY16 mixing period was 371.8 ms. The duration of the 180° pulse and the delay between the 180° pulses were 30.5 and 260 μs, respectively. The $^{1}H^{N}$ chemical shift of E18 is 8.70 ppm

The experiments with the MOCCA-XY16 isotropic mixing scheme for a long period correlated additional cross resonances with $^{15}N_{i-2}$ and $^{15}N_{i+2}$ frequencies in the extracted trace of the *i*-th amide group (Fig. 10b). Furthermore, cross resonances with $^{15}N_{i-3}$ and $^{15}N_{i+3}$ frequencies were observed for some amide groups (Fig. 10c, d), establishing connectivity of a total of seven residues simultaneously. The 3D (HN)CO(CO)NH experiments also correlated up to seven adjacent carbonyl carbon nuclei (Fig. 10e). The 3D (H)N(COCO)NH spectrum was also recorded at 17.6 T with the mixing period of 537 ms (Fig. 10f). Although the decay of the spin coherence during the MOCCA-XY16 sequence is about 1.3-fold faster at 17.6 T than at 11.7 T (Fig. 4b), many cross resonances can be detected. The results suggest that 3D (H)N(COCO)NH and (HN)CO(CO)NH schemes with MOCCA-XY16 are powerful tools for sequential assignment of IDPs.

Sequential connectivity across proline residues

Sequential connectivity, based on (^{1}H,^{15}N)-resolved triple resonance experiments, is interrupted by proline residues due to lack of the amide protons. Proline residues are often abundant in IDPs, which complicates sequential resonance assignments of IDPs. In 3D (H)N(COCO)NH and (HN)CO(CO)NH schemes with a long mixing period, however, resonances of residues *i* and $i \pm 2$ can be connected across the proline residue. An example is shown in Fig. 11. Due to sequential magnetization transfer through $^{13}C'$ between A107 and Q109, the connectivity pattern is not interrupted by P108.

Alternatively, the resonances involving proline residues can be detected by use of ^{13}C-start or ^{13}C-detection experiments. Figure 12 shows a comparison between the ^{1}H-start and ^{13}C-start 2D experiments performed on ubiquitin, where the magnetization transfer can be respectively described as:

$$^{1}H^{N} \rightarrow {}^{15}N^{H}(t_1) \rightarrow {}^{13}C' \rightarrow {}^{13}C' \,(\text{mixing}) \rightarrow {}^{15}N^{H} \rightarrow {}^{1}H^{N}(t_3) \quad (7a)$$

$$^{13}C' \rightarrow {}^{15}N^{H}(t_1) \rightarrow {}^{13}C' \rightarrow {}^{13}C' \,(\text{mixing}) \rightarrow {}^{15}N^{H} \rightarrow {}^{1}H^{N}(t_3) \quad (7b)$$

While the ^{15}N chemical shift of P19 was missing in the ^{1}H-start experiment (Fig. 12a), ^{13}C direct polarization allowed for detection of the relevant resonance (Fig. 12b). When solvent exchange due to exposure of the amide groups to the solvent causes line broadening of the resonances beyond detection, ^{13}C direct detection experiments are ideal because carbonyl nuclei are not influenced by exchange broadening (Balayssac et al. 2006; Bermel et al. 2005, 2006; Felli and Pierattelli 2014).

Sequential connectivity of backbone resonances of intrinsically disordered proteins

Figure 13 shows strip plots from a 3D (H)N(COCO)NH experiment on αSyn at 11.7 T with MOCCA-XY16 isotropic mixing for 393 ms. The strip plots show sequential connectivity for the amide resonances from S9 to A19. Although application of carbonyl–carbonyl correlation NMR experiments for resonance assignments of IDPs was reported previously (Bermel et al. 2006; Liu et al. 2000), a significant advantage here is that the strips include a diagonal resonance ($^{15}N_i$) and four cross resonances ($^{15}N_{i-2}$, $^{15}N_{i-1}$, $^{15}N_{i+1}$, and $^{15}N_{i+2}$).

In conclusion, we demonstrate here that 3D (H)N(COCO)NH and (HN)CO(CO)NH experiments with the MOCCA-XY16 mixing scheme can be used to correlate backbone $^{15}N^{H}$ and $^{13}C'$ nuclei by scalar transfer over as many as 18 chemical bonds. High-resolution spectra can be obtained by semi-constant time chemical shift evolution and ^{1}H decoupling during $^{13}C'$ chemical shift evolution. As

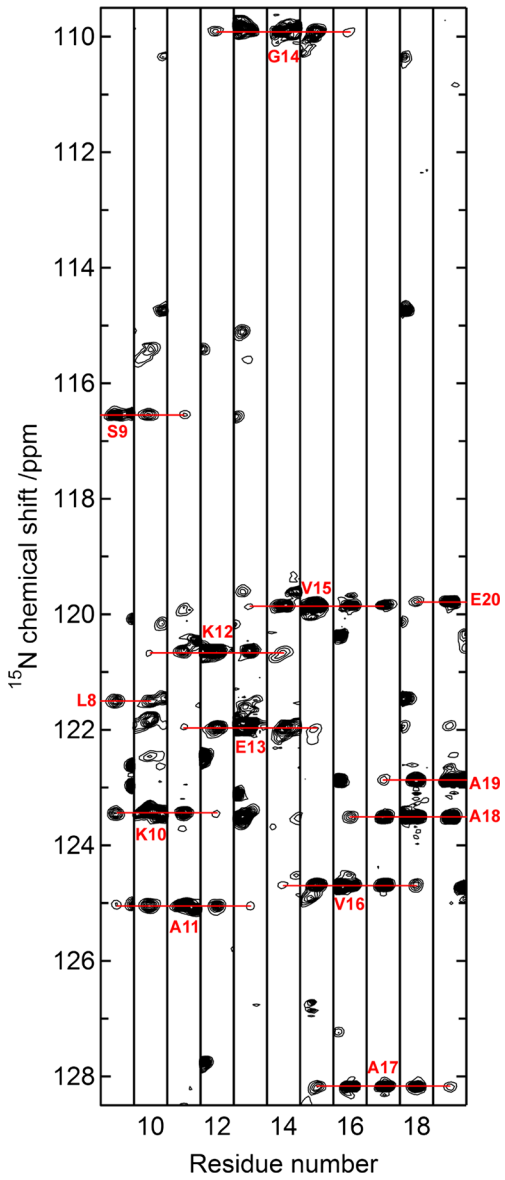

Fig. 13 Strip plots for the N-terminal residues (from S9 to A19) of uniformly ^{13}C,^{15}N-labelled αSyn from 3D (H)N(COCO)NH experiments at the magnetic field of 11.7 T with MOCCA-XY16 isotropic mixing for 393 ms

relaxation losses are efficiently mitigated by the MOCCA-XY16 mixing scheme, the experiment was also shown to work at higher magnetic fields. Multiple, recurrent long-range correlations with ultra-high resolution lift the close chemical shift degeneracy of the backbone nuclei in disordered proteins, and allow all the backbone ^{1}H^{N}, ^{15}N^{H}, and ^{13}C′ resonance assignments to be assigned *de novo* from a single pair of 3D experiments.

Acknowledgments We thank Camilla B. Andersen and Tania A. Nielsen (Aarhus University, Denmark) for the expression and purification of αSyn and ubiquitin, respectively. Y.Y. is supported by an EMBO Long-Term Fellowship (ALTF 687-2013).

References

Balayssac S, Jimenez B, Piccioli M (2006) ^{13}C direct detected COCO-TOCSY: a tool for sequence specific assignment and structure determination in *protonless* NMR experiments. J Magn Reson 182:325–329

Bermel W, Bertini I, Duma L, Felli IC, Emsley L, Pierattelli R, Vasos PR (2005) Complete assignment of heteronuclear protein resonances by protonless NMR spectroscopy. Angew Chem Int Ed 44:3089–3092

Bermel W, Bertini I, Felli IC, Lee YM, Luchinat C, Pierattelli R (2006) Protonless NMR experiments for sequence-specific assignment of backbone nuclei in unfolded proteins. J Am Chem Soc 128:3918–3919

Bermel W, Bertini I, Felli IC, Gonnelli L, Kozminski W, Piai A, Pierattelli R, Stanek J (2012) Speeding up sequence specific assignment of IDPs. J Biomol NMR 53:293–301

Buevich AV, Baum J (1999) Dynamics of unfolded proteins: incorporation of distributions of correlation times in the model free analysis of NMR relaxation data. J Am Chem Soc 121:8671–8672

Buevich AV, Shinde UP, Inouye M, Baum J (2001) Backbone dynamics of the natively unfolded pro-peptide of subtilisin by heteronuclear NMR relaxation studies. J Biomol NMR 20:233–249

Camilloni C, De Simone A, Vranken WF, Vendruscolo M (2012) Determination of secondary structure populations in disordered states of proteins using nuclear magnetic resonance chemical shifts. Biochemistry 51:2224–2231

Chang SL, Tjandra N (2005) Temperature dependence of protein backbone motion from carbonyl ^{13}C and amide ^{15}N NMR relaxation. J Magn Reson 174:43–53

Clubb RT, Thanabal V, Wagner G (1992) A constant-time three-dimensional triple-resonance pulse scheme to correlate intraresidue ^{1}H^{N}, ^{15}N, and ^{13}C′ chemical shifts in ^{15}N–^{13}C-labeled proteins. J Magn Reson 97:213–217

Delaglio F, Grzesiek S, Vuister GW, Zhu G, Pfeifer J, Bax A (1995) NMRPipe: a multidimensional spectral processing system based on UNIX pipes. J Biomol NMR 6:277–293

Engelke J, Ruterjans H (1997) Backbone dynamics of proteins derived from carbonyl carbon relaxation times at 500, 600 and 800 MHz: application to ribonuclease T1. J Biomol NMR 9:63–78

Felli IC, Pierattelli R (2014) Novel methods based on ^{13}C detection to study intrinsically disordered proteins. J Magn Reson 241:115–125

Felli IC, Pierattelli R, Glaser SJ, Luy B (2009) Relaxation-optimised Hartmann–Hahn transfer using a specifically Tailored MOCCA-XY16 mixing sequence for carbonyl–carbonyl correlation spectroscopy in ^{13}C direct detection NMR experiments. J Biomol NMR 43:187–196

Furrer J, Kramer F, Marino JP, Glaser SJ, Luy B (2004) Homonuclear Hartmann–Hahn transfer with reduced relaxation losses by use of the MOCCA-XY16 multiple pulse sequence. J Magn Reson 166:39–46

Giehm L, Svergun DI, Otzen DE, Vestergaard B (2011) Low-resolution structure of a vesicle disrupting α-synuclein oligomer that accumulates during fibrillation. Proc Natl Acad Sci U S A 108:3246–3251

Grzesiek S, Bax A (1992) Correlating backbone amide and side chain resonances in larger proteins by multiple relayed triple resonance NMR. J Am Chem Soc 114:6291–6293

Grzesiek S, Bax A (1993) Amino acid type determination in the sequential assignment procedure of uniformly ^{13}C/^{15}N-enriched proteins. J Biomol NMR 3:185–204

Grzesiek S, Bax A (1997) A three-dimensional NMR experiment with improved sensitivity for carbonyl–carbonyl J correlation in proteins. J Biomol NMR 9:207–211

Hu JS, Bax A (1996) Measurement of three bond ^{13}C–^{13}C *J* couplings between carbonyl and carbonyl/carboxyl carbons in isotopically enriched proteins. J Am Chem Soc 118:8170–8171

Ikura M, Kay LE, Bax A (1990) A novel approach for sequential assignment of proton, carbon-13, and nitrogen-15 spectra of larger proteins: heteronuclear triple-resonance three-dimensional NMR spectroscopy. Application to calmodulin. Biochemistry 29:4659–4667

Kadkhodaie M, Rivas O, Tan M, Mohebbi A, Shaka AJ (1991) Broadband homonuclear polarization using flip–flop spectroscopy. J Magn Reson 91:437–443

Kay LE, Keifer P, Saarinen T (1992) Pure absorption gradient enhanced heteronuclear single quantum correlation spectroscopy with improved sensitivity. J Am Chem Soc 114:10663–10665

Kay LE, Xu GY, Yamazaki T (1994) Enhanced-sensitivity triple-resonance spectroscopy with minimal H_2O saturation. J Magn Reson A 109:129–133

Kjaergaard M, Poulsen FM (2012) Disordered proteins studied by chemical shifts. Prog Nucl Magn Reson Spectrosc 60:42–51

Kosol S, Contreras-Martos S, Cedeno C, Tompa P (2013) Structural characterization of intrinsically disordered proteins by NMR spectroscopy. Molecules 18:10802–10828

Kramer F, Peti W, Griesinger C, Glaser SJ (2001) Optimized homonuclear Carr–Purcell-type dipolar mixing sequence. J Magn Reson 149:58–66

Lipari G, Szabo A (1982a) Model-free approach to the interpretation of nuclear magnetic resonance relaxation in macromolecules. 1. Theory and range of validity. J Am Chem Soc 104:4546–4559

Lipari G, Szabo A (1982b) Model-free approach to the interpretation of nuclear magnetic resonance relaxation in macromolecules. 2. Analysis of experimental results. J Am Chem Soc 104:4559–4570

Liu A, Riek R, Wider G, von Schroetter C, Zahn R, Wüthrich K (2000) NMR experiments for resonance assignments of ^{13}C, ^{15}N doubly-labeled flexible polypeptides: application to the human prion protein hPrP(23–230). J Biomol NMR 16:127–138

Logan TM, Olejniczak ET, Xu RX, Fesik SW (1993) A general method for assigning NMR spectra of denatured proteins using 3D HC(CO)NH-TOCSY triple resonance experiments. J Biomol NMR 3:225–231

Maltsev AS, Ying J, Bax A (2012) Deuterium isotope shifts for backbone ^{1}H, ^{15}N and ^{13}C nuclei in intrinsically disordered protein and α-synuclein. J Biomol NMR 54:181–191

Marion D, Ikura M, Tschudin R, Bax A (1989) Rapid recording of 2D NMR spectra without phase cycling. Application to the study of hydrogen exchange in proteins. J Magn Reson 85:393–399

Markley JL, Bax A, Arata Y, Hilbers CW, Kaptein R, Sykes BD, Wright PE, Wuthrich K (1998) Recommendations for the presentation of NMR structures of proteins and nucleic acids. IUPAC–IUBMB–IUPAB inter-union task group on the standardization of data bases of protein and nucleic acid structures determined by NMR spectroscopy. J Biomol NMR 12:1–23

Markwick PR, Sattler M (2004) Site-specific variations of carbonyl chemical shift anisotropies in proteins. J Am Chem Soc 126:11424–11425

Motackova V, Novacek J, Zawadzka-Kazimierczuk A, Kazimierczuk K, Zidek L, Sanderova H, Krasny L, Kozminski W, Sklenar V (2010) Strategy for complete NMR assignment of disordered proteins with highly repetitive sequences based on resolution-enhanced 5D experiments. J Biomol NMR 48:169–177

Mulder FAA, Lundqvist M, Scheek RM (2010) Nuclear magnetic resonance spectroscopy applied to (intrinsically) disordered proteinsin. In: Uversky VN, Longhi S (eds) Instrumental analysis of intrinsically disordered proteins: assessing structure and conformation. Wiley, Hoboken, pp 61–87

Mulder FAA, Otten R, Scheek RM (2011) Origin and removal of mixed-phase artifacts in gradient sensitivity enhanced heteronuclear single quantum correlation spectra. J Biomol NMR 51:199–207

Novacek J, Zidek L, Sklenar V (2014) Toward optimal-resolution NMR of intrinsically disordered proteins. J Magn Reson 241:41–52

Sattler M, Schleucher J, Griesinger C (1999) Heteronuclear multidimensional NMR experiments for the structure determination of proteins in solution employing pulsed field gradients. Prog Nucl Magn Reson Spectrosc 34:93–158

Schwarzinger S, Kroon GJ, Foss TR, Chung J, Wright PE, Dyson HJ (2001) Sequence-dependent correction of random coil NMR chemical shifts. J Am Chem Soc 123:2970–2978

Shaka AJ, Lee CJ, Pines A (1988) Iterative schemes for bilinear operatiors; application to spin decoupling. J Magn Reson 77:274–293

Tamiola K, Mulder FAA (2012) Using NMR chemical shifts to calculate the propensity for structural order and disorder in proteins. Biochem Soc Trans 40:1014–1020

Tamiola K, Acar B, Mulder FAA (2010) Sequence-specific random coil chemical shifts of intrinsically disordered proteins. J Am Chem Soc 132:18000–18003

Uversky VN (2011) Intrinsically disordered proteins from A to Z. Int J Biochem Cell Biol 43:1090–1103

Uversky VN, Fink AL (2004) Conformational constraints for amyloid fibrillation: the importance of being unfolded. Biochim Biophys Acta 1698:131–153

Wang T, Cai S, Zuiderweg ERP (2003) Temperature dependence of anisotropic protein backbone dynamics. J Am Chem Soc 125:8639–8643

Wishart DS, Bigam CG, Holm A, Hodges RS, Sykes BD (1995) ^{1}H, ^{13}C and ^{15}N random coil NMR chemical shifts of the common amino acids. I. Investigations of nearest-neighbor effects. J Biomol NMR 5:67–81

Wright PE, Dyson HJ (1999) Intrinsically unstructured proteins: re-assessing the protein structure-function paradigm. J Mol Biol 293:321–331

Yao J, Dyson HJ, Wright PE (1997) Chemical shift dispersion and secondary structure prediction in unfolded and partly folded proteins. FEBS Lett 419:285–289

Ying J, Roche J, Bax A (2014) Homonuclear decoupling for enhancing resolution and sensitivity in NOE and RDC measurements of peptides and proteins. J Magn Reson 241:97–102

Yuwen T, Skrynnikov NR (2014a) CP-HISQC: a better version of HSQC experiment for intrinsically disordered proteins under physiological conditions. J Biomol NMR 58:175–192

Yuwen T, Skrynnikov NR (2014b) Proton-decoupled CPMG: a better experiment for measuring ^{15}N R_2 relaxation in disordered proteins. J Magn Reson 241:155–169